IBIS/PICsIT

Instrument Specific Software (ISSW)

Report on the Scientific Performances of the PICsIT ISSW

Version: 1.2 – Date: 27 October 2003

Responsible: Luigi Foschini
IASF–CNR, Sezione di Bologna, (Italy)
email: foschini@bo.iasf.cnr.it
email: foschini@isdcmail.unige.ch

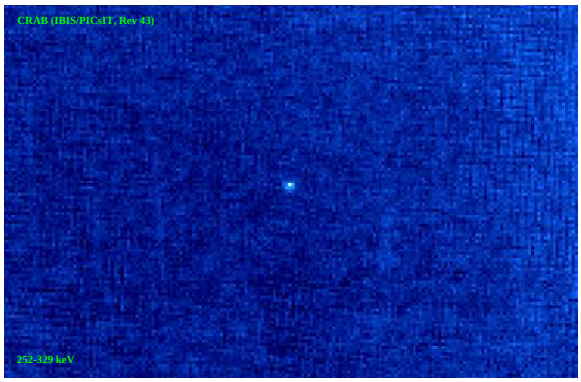

	Revision History
v 1.0	First version for first software release of March 2003.
28/02/2003	
v 1.1	Update for the intermediate software release of May 2003.
30/04/2003	Early analysis of Cyg X–1, cleaning of cosmic–ray induced events, improvement of the position accuracy, comparison with ECOE data.
v 1.2	Update for OSA 3 release.
27/10/2003	Crab in rev 102; automatic source location; timing analysis. Some error corrected. Removed the non–standard analysis section.

Cover picture: Crab observed by PICsIT on 19 February 2003 for 132 ks in the energy band $252 - 329$ keV.

1 What is now available

This report summarizes the scientific performances and reliability of the Instrument Specific Software (ISSW) of the PICsIT detector layer of the IBIS imager. The executables analysed here are those officially delivered to date (27 October 2003), together with their Instrument Configuration (IC) files. The PICsIT–ISSW delivered to date for the Scientific Analysis of the PICsIT data include:

- `ibis_pics_deadtime` (v 2.1, 23 October 2002): to calculate the intrinsic deadtime of the detector. It works well; no particular problem after the launch.

- `ip_ev_correction` (v 1.6, 14 November 2002): to perform a correction of gain and offset variations in addition to those performed on board by the Instrument Application Software (IASW). It is for data obtained in photon–by–photon mode. It is strilctly linked with the IC data structure PICS–ENER–MOD, containing the average gain, offset, and the deviations from these values pixel by pixel. The latest version of PICS–ENER–MOD is dated 30 October 2002 and was built by using the data in the IBIS Scientific Performance Report (IBIS Calibration Team, 2002). A new table in under preparation, to make full use of the analysis of the in–flight behaviour (Malaguti et al. 2003a). The exectuable is now stable and working. The only expected changes concerns the IC file, that should be updated with in flight data.

- `ip_ev_shadow_build` (v 2.2, 22 April 2003): to perform the building of the shadowgrams and the efficiency maps from data in photon–by–photon mode. It is stable and working. The only missing part is the treatment of the Good Time Interval (GTI); however, since the photon–by–photon mode is not the standard mode for PICsIT, and it was used only in exceptional cases during the PV phase with dedicated telemetry (because of the high background), the GTI inclusion is a low priority task. The executable is already ready to prepare shadowgrams also for the spectra extraction. Recently, the algorithm to clean the spurious events induced by cosmic-rays has been introduced (it works on `IBIS mode`= 43). See Sect. 2.2 for more details.

- `ip_si_shadow_build` (v 2.7, 10 June 2003): to perform the building of shadowgrams and the efficiency maps from the data in standard mode

(spectral imaging). It is stable and working. It is worth mentioning that the executable now deals with complete or partially complete histograms. If histograms are not complete, the executable returns simply a warning, but it continues the analysis. The missing pixels will be trated as killed pixels. The executable is already ready to prepare shadowgrams also for the spectra extraction.

- `ip_shadow_ubc` (v 2.4, 25 February 2003): to perform the correction for background and detector non–uniformities. The output shadowgrams are also expanded to take into account the gaps between modules. The gaps and the killed pixels are filled with a mean value. There is also a variance map, calculated starting from the statistical variance of the detector counts and updated according to the correction performed. The executable is linked with the following IC data structures: PICS–SBAC–BKG (background maps for single events), PICS–MBAC–BKG (background maps for multiple events), PICS–SUNI–BKG (detector non–uniformities for single events), and PICS–MUNI–BKG (detector non–uniformities for multiple events). See Sect. 2.1 for details.

- `ip_skyimage` (v 2.4.1, 22 October 2003): it performs the deconvolution and sky image reconstruction by means of the algorithm described by Goldwurm et al. (2003). The executable is working, producing a basic deconvolved sky image, variance, and significance maps. It performs also the automatic source location for staring observation. See Sect. 3 for details.

- `ip_st_lc_extract` (v 2.2, 11 September 2003): it performs the extraction of the lightcurve of the whole detector from the spectral timing data. The barycentric correction is applied, by using the library DAL3AUX. The executable is stable and working. The output files are in compliance with OGIP standards([1]).

- `Additional notes`: The executable for the Automatic Calibration Analysis (ACA) is not yet completed, because it is necessary to wait for an analysis of in–flight variations of the gains. After this analysis, it will be decided if this executable is necessary or not. The executables for the extraction of the spectrum and lightcurves from point–like

[1]See http://heasarc.gsfc.nasa.gov/docs/heasarc/ofwg/ofwg_recomm.html

sources are not yet ready. Work is in progress. Moreover, the PICsIT ISSW makes use of other executables when inserted into the IBIS pipeline (GTI, Catalog Extraction, and so on...). These executables are made by ISDC and are not analysed here directly, although the proper working of these modules is essential to have the full OSA for PICsIT.

More details on some single items are in the following sections.

2 The correction for background

2.1 Maps

There are no detector non–uniformities map available to date, except of one map created for test purposes (single events; no energy selection). The map is not to be used with the actual version of the ISSW, since it has been written with an old template, no more used. Using this map, can give wrong results and the crash of the pipeline. The removal of these maps from the archive has been requested.

For the background maps, the situation is different: there are three useful sets, prepared from the empty field observations of the revolution 13 (1 set for single and multiple events; 8 energy bands) and 38 (2 sets for single and multiple events; 8 energy bands). The differences in the two sets from the revolution 38 are due to a change in the energy bands.

PICsIT operates in an energy region dominated by the background (that is also higher than expected from numerical models – cf Ferguson et al. 2003), where we expect that the source counts are of the order of 1% of the global counts detected. This means that the background subtraction is of fundamental importance for the instrument capabilities.

The availability to date of only the empty field observations does not allow the user to be free to select the energy bands to produce images. A set of default energy bands has been created to have the best source statistics, with the lowest possible contamination from background or other events, such as the cosmic–rays induced events (see Segreto et al. 2003). These energy bands, prepared by G. Di Cocco and G. Malaguti, are shown in Table 1.

A set of background maps corresponding to the energy bands listed in Table 1 have been created by means of the empty field observations of revolution 38. Only about 13 ks (single events) and less than 9 ks (multiple

Table 1: PICsIT Energy Bands. Columns: (1) Channel number in photon–by–photon mode; (2) Channel number in standard mode; (3) Energy [keV].

Channels PPM (1)	Channels Standard (2)	Energy (3)
Single Events		
29 – 35	10 – 16	203 – 252
36 – 46	17 – 27	252 – 329
47 – 64	28 – 41	329 – 455
65 – 94	42 – 56	455 – 655
95 – 150	57 – 84	655 – 1057
151 – 262	85 – 140	1057 – 1841
263 – 509	141 – 196	1841 – 3570
510 – 929	197 – 254	3570 – 6510
Multiple Events		
24 – 31	5 – 12	336 – 448
32 – 46	13 – 27	448 – 658
47 – 74	28 – 46	658 – 1050
75 – 130	47 – 74	1050 – 1834
131 – 254	75 – 136	1834 – 3570
255 – 464	137 – 187	3570 – 6510
465 – 679	188 – 229	6510 – 9520
680 – 929	230 – 254	9520 – 13020

events) of empty field observations were available and used to produce background maps. No corresponding detector uniformity maps have been created, since a modelling activity is necessary to separate the contribution of the background from the detector non–uniformities. With the empty field observations is only possible to subtract the background. Nevertheless, this correction, although partial, is sufficient for the moment. At least, it is possible to obtain useful images for integration time scale of 1 revolution. For longer exposures, the background noise can increase too much. More detailed maps are under study.

It is worth mentioning, as already seen in SIGMA calibrations and data reduction (Bouchet et al. 2001), that a background subtraction is more efficient when the background map is prepared from a nearby observation. This means that the background map generation is continuosly evolving.

Presently the executable contains two ways to rescale the background maps: according to the time of exposure and to the average value of counts.

Although a more detailed study is necessary, it appears that the average value scaling could give better results. The distribution of significance values in the pixels of the field of view during the Crab observation of calibration is generally a gaussian, with a peak close to 0. A residual of $\pm 0.2\sigma$ is sometimes present. This systematic error will be corrected in the future versions of the software.

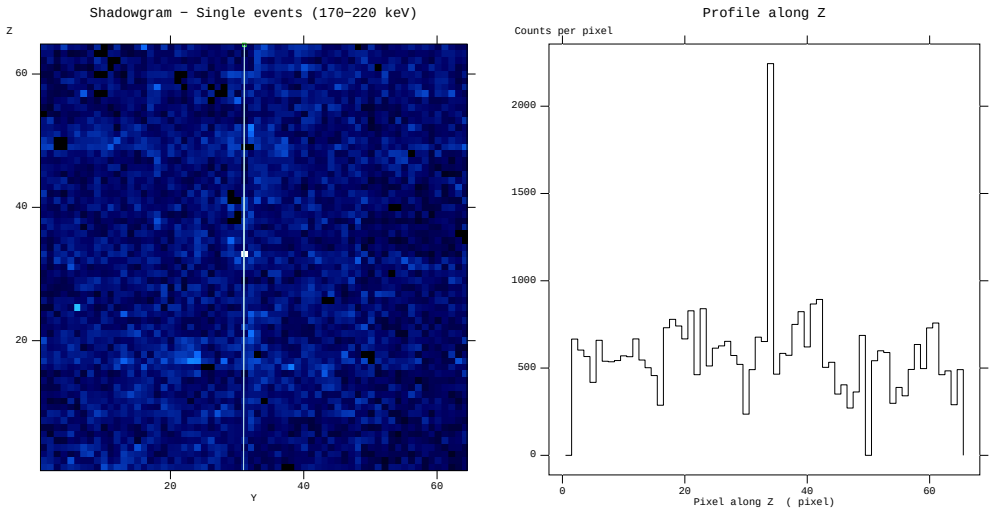

Figure 1: Effect of cosmic-rays induced events on the shadowgrams. The white pixels have an anomalous high count value. This example is taken from the data of revolution 24 in the energy band $170 - 220$ keV; PICsIT was in photon–by–photon mode.

2.2 Cosmic–ray induced events

Since the beginning of the in–flight operations, it was clear that there were spurious events contaminating the detector in addition to the backgroud and source events([2]). The cause was identified in cosmic–ray induced events, that are roughly the 10% of the total events and affect mainly the energy bands below 300 keV (Segreto et al. 2003, see also Natalucci 2003). As underlined by Natalucci (2003) these fake events can significanly affect the

[2]See some nice animations by the IBIS Team in Tübingen at http://astro.uni–tuebingen.de/groups/integral/anim_gif/.

performances of PICsIT. However, it is possible to perform a cleaning only in photon–by–photon mode. In standard mode, it is possible to perform only an *a posteriori* correction: when the pixel counts are higher than a constant multiplied by the average count values, i.e. $counts > k \cdot average$ (see Fig. 1), then it is assumed that this abnormal high value is due to a cosmic–ray induced event and the pixel value is reset to the mean value. First tests showed a certain effectiveness of this correction, but work is in progress to have a better solution, according to the casual nature of these events.

This hypothesis is confirmed by the analysis of photon–by–photon data: indeed, in this case, it was possible to develop an algorithm to delete from the photon list those events that can be identified as fake. After having isolated some of these "tracks", the photon list displayed series of photons "packed" in a very short time scale hitting a single pixel. Such "packets" are shown in Fig. 2, where fake events are emphasized in blue.

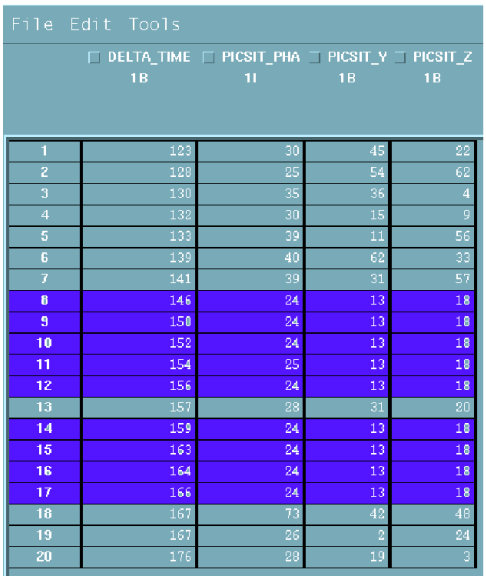
File Edit Tools

	DELTA_TIME 1B	PICSIT_PHA 1I	PICSIT_Y 1B	PICSIT_Z 1B
1	123	30	45	22
2	128	25	54	62
3	130	35	36	4
4	132	30	15	9
5	133	39	11	56
6	139	40	62	33
7	141	39	31	57
8	146	24	13	18
9	150	24	13	18
10	152	24	13	18
11	154	25	13	18
12	156	24	13	18
13	157	28	31	20
14	159	24	13	18
15	163	24	13	18
16	164	24	13	18
17	166	24	13	18
18	167	73	42	48
19	167	26	2	24
20	175	28	19	9

Figure 2: Identification in the photon list (single events) of fake events produced by cosmic–rays. Spurious events are emphasized in blue.

By removing these packets it is possible to obtain a cleaned shadowgram (Fig. 3), but obviously this is possible only when PICsIT is set to operate in photon–by–photon mode. Since the available telemetry is not sufficient for

this type of operation, PICsIT will work almost always in standard mode, i.e. with events integrated onboard in histograms. In this way, there is no possibility to act on the single photon and it is possible only to operate the *a posteriori* correction described above.

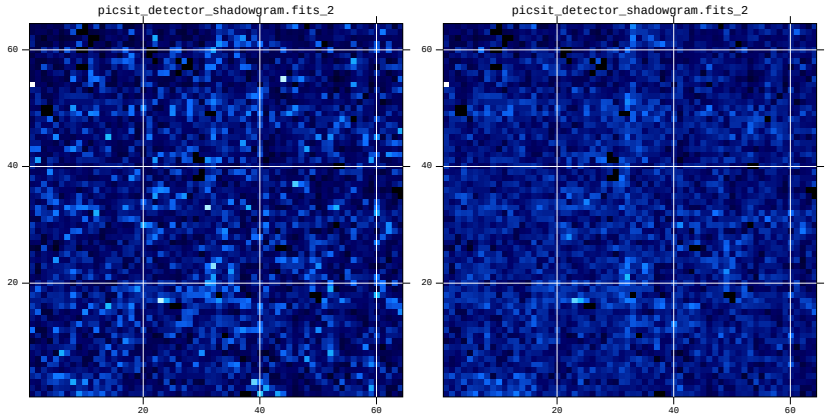

Figure 3: Effect of cosmic–rays induced events on the shadowgrams. (*left*) Normal shadowgram; (*right*) Cleaned shadowgram. After the cleaning, the bright pixels disappeared. The only bright pixel remained at the top left of the cleaned shadowgram is a well–known pixel that often is noisy. Data from revolution 14, energy band $170 - 250$ keV.

3 The sky image reconstruction

Here are shown some performances of the PICsIT ISSW. Details on the techniques of the deconvolution are available in Goldwurm et al. (2003).

3.1 Sky coordinates reconstruction

The sensitivity of PICsIT does not allow to see sources during a typical exposure of one ScW ($2-5$ ks). It is necessary to integrate the shadowgrams to obtain long exposures of the order of 10^4-10^5 s. This resulted to be problematic in realizing a detailed and extensive study of misalignement. Therefore the correction for systematic effects in the sky coordinates reconstructions has been performed in two phases: during the first phase (from the PV phase

to July 2003), the misalignement matrix was set equal to the identity and a correction was applied directly in the deconvolution module (`ip_skyimage`) in order to minimize the offset with the Crab position. During the second phase (from July 2003), the misalignement matrix of PICsIT has the same values of that of ISGRI, since it is expected that the misalignement of the two layers are equal (cf Walter et al. 2003). The correction performed in the deconvolution module has been removed from the version 2.4.

Table 2: Source position accuracy. Columns: (1) Source name; (2) Reference position (RA, Dec, J2000) from catalog or circulars; (3) PICsIT position (RA, Dec, J2000); (4) Offset [arcmin]. The position for PICsIT are taken in the 252 – 329 keV energy band. The two positions for the GRB refers to that from the plain deconvolution (*Plain*) and that after the interpolation (*Int*).

Source	Reference Position	PICsIT Position	Offset
(1)	(2)	(3)	(4)
Cygnus X–1	19 : 58 : 22; +35 : 12 : 06	19 : 58 : 08; +35 : 08 : 40	4.4′
Crab Star	05 : 34 : 32; +22 : 00 : 52	05 : 34 : 13; +21 : 55 : 48	6.8′
Crab Star Int (*)		05 : 34 : 33; +21 : 59 : 13	1.7′
Crab Dith		05 : 34 : 24; +22 : 01 : 20	1.9′
Crab Off Ax		05 : 34 : 17; +21 : 59 : 11	3.8′
GRB 021125 Int	19 : 47 : 56, +28 : 23 : 28	19 : 47 : 46, +28 : 17 : 14	6.6′
GRB 021125 Plain		19 : 47 : 34, +28 : 15 : 13	9.5′

To date, only three sources are available to test the sky coordinates reconstruction: they are Cygnus X–1 and Crab – in the FCFOV – and GRB021125 – in the PCFOV – (Bazzano and Paizis 2002). The position of the Crab and Cygnus X–1 can be checked with the known catalog position, e.g. Simbad. For the GRB there can be the problem that the only position available with sufficient precision is that obtained with ISGRI (Gros and Produit 2002), the low–energy detector layer of IBIS, and there is the risk of self–reference. But the follow–up with other satellites of the GCN (GRB Coordinates Network) confirmed the position.

In the Table 2 are reported the positions found and the comparison with the other known coordinates. The positions marked with (*) is the output from the automatic source detection for staring observations and with the misalignement matrix of July 2003. All the others refers to the early phase,

with the identity misalignement matrix and the correction in the deconvolution.

The three positions for the Crab are obtained from the staring observation during the revolution 39 (Crab Star, 77 ks), from dithering osbervation of the revolution 43 (Crab Dith, 132 ks), and from Crab off–axis of 0.5° from the revolution 44 (Crab Off Ax, 104 ks). The position for Cyg X–1 is obtained from the dithered observation of revolution 11 (80 ks).

The fact that PICsIT shows the best results in the energy band $252 - 329$ keV can be due to the fact that this band is sufficiently low to have enough photons, but also sufficiently high to be not so much affected by the cosmic-ray induced events.

The worst cases are for the Crab in staring and for the GRB (but this is in the PCFOV). However, it is worth noting that one pixel of PICsIT corresponds to about $10'$, so that an offset of $6.6'$ corresponds just to about half a pixel.

4 Imaging with the calibration sources

4.1 Crab

For the analysis with the Crab were selected the data from the revolution 39 (Crab on axis, staring, 77 ks), 43 (Crab on axis, dithering, 132 ks), and 44 (Crab off axis of 0.5°, dithering, 104 ks), and 102 (Crab on axis, dithering, 47 ks). The results are shown in the Table 3.

Table 3: PICsIT observations of the Crab during Rev. 39 (staring, on axis, 77 ks), Rev. 43 (dithering, on axis, 132 ks), Rev. 44 (dithering, off axis 0.5°, 104 ks), Rev. 102 (dithering, on axis, 47 ks). The columns indicate the energy band [keV], the count rate in the peak pixel [c/s] and the significance of the detection for each revolution.

	Rev 39		Rev 43		Rev 44		Rev 102	
Energy Band	Rate	σ	Rate	σ	Rate	σ	Rate	σ
$200 - 252$	2.5	7.4	1.5	5.9	3.1	5.7	1.8	2.7
$252 - 329$	2.2	11.0	2.1	10.0	2.6	8.0	2.3	6.4
$329 - 455$	1.3	7.1	1.2	6.5	1.4	5.0	1.1	3.5
$455 - 655$	0.7	4.4	0.6	3.3	0.6	3.0	0.6	2.3

Monte Carlo simulations by Del Santo et al. (2001) are available for comparison, although in different energy bands (Table 4).

Table 4: Monte Carlo simulations of PICsIT observations of the Crab. Columns: (1) Energy band [keV]; (2) Count rate [c/s].

Energy Band (1)	Rate (2)
$150-250$	10
$250-400$	4.6
$400-1000$	2.1

The best performances of PICsIT are obtained in the energy band $252-329$ keV, that is less affected by the cosmic–rays induced events and is in a range sufficiently low to detect enough photons. In the Fig. 4-6 are shown the significance maps of the observation at $252-329$ keV, the best detection, together with the radial profile.

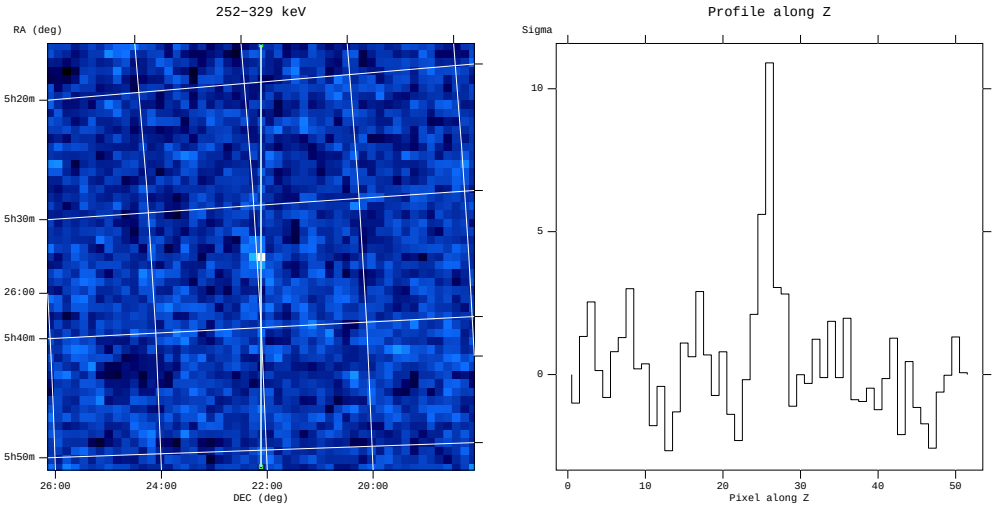

Figure 4: Crab observation during the rev 39 (staring, on axis, 77 ks). Significance map and profile in the energy band $252-329$ keV.

The greatest differences in the count rates and significance (for observations in staring, dithering, off axis) occur just the band $203-252$ keV, where

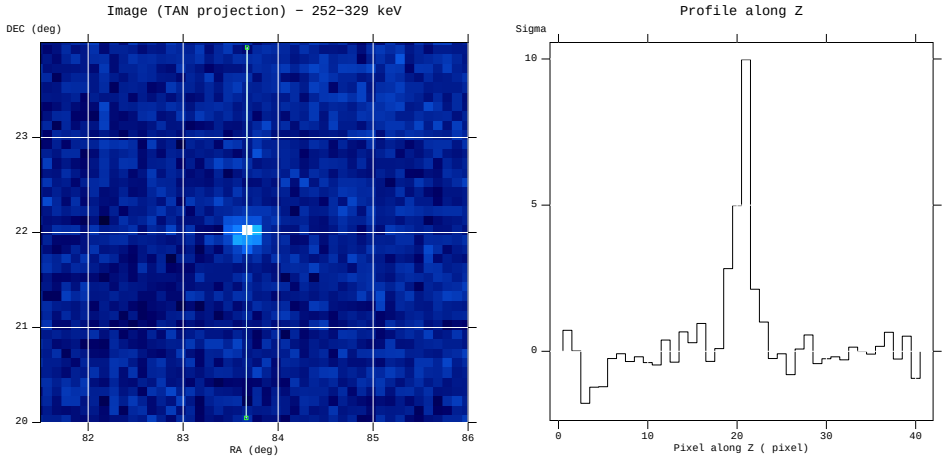

Figure 5: Crab observation during the rev 43 (dithering, on axis, 132 ks). Significance map and profile in the energy band $252 - 329$ keV.

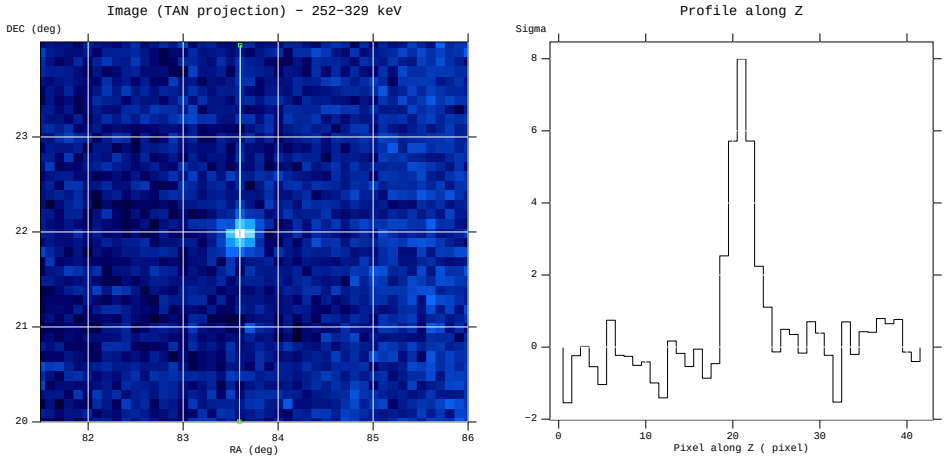

Figure 6: Crab observation during the rev 44 (dithering, off axis (0.5°), 104 ks). Significance map and profile in the energy band $252 - 329$ keV.

we expect that the impact of cosmic–ray induced events is still high and the *a posteriori* correction – the only available since PICsIT is operated in histogram mode – for the cosmic–rays induced events may not be too much accurate (see Sect. 2.2).

In addition, we expect to have a degradation of the performances of the instrument when we change mode of observation (staring to dithering) or when we have the source off axis. To evaluate this, the three observations of the Crab (staring, dithering, dithering and off axis) have been normalized to the exposure of 132 ks (Table 5). Although it is expected that the value are a bit lower when passing from staring to dithering, since the mosaic performs an interpolation (pixels are not always perfectly aligned), this can account of only for a difference of 10%. Therefore, the greater differences shown in Table 5 are mostly due to other factors. The most probable cause is when PICsIT is used in dithering, since IBIS has a mask best suited to work in staring. It is worth noting, that these are preliminary results and should be confirmed with more tests.

Table 5: PICsIT normalized observations of the Crab during Rev. 39 (staring, on axis, 77 ks), Rev. 43 (dithering, on axis, 132 ks), Rev. 44 (dithering, off axis 0.5°, 104 ks). The columns indicate the energy band [keV] and the significance of the detection for each revolution. The significance has been rescaled to the 132 ks of exposure of rev 43.

	Rev 39	Rev 43	Rev 44
Energy Band	σ	σ	σ
$200 - 252$	9.6	5.9	6.4
$252 - 329$	14.3	10.0	9.0
$329 - 455$	9.2	6.5	5.6
$455 - 655$	5.7	3.3	3.4

4.2 Cygnus X–1

Soon after the launch of INTEGRAL (17 October 2002), it was not possible to observe the Crab, since it was too close to the Sun. Therefore, Cygnus X–1 was selected as calibration source. The first observations started during the revolution 11 and PICsIT was in standard mode.

For other reasons, it was not possible to analyse immediately Cygnus X–1, but now – with the consolidated data – it is possible. To date the revolution 11 (80 ks, dithering) and 12 (13 ks, staring) have been analysed, with the detection of Cygnus X–1 in the first three energy bands of the observation in revolution 11. The 13 ks of the revolution 12 were not sufficient for a detection. The best detection is shown in Fig. 7. Since at that time there

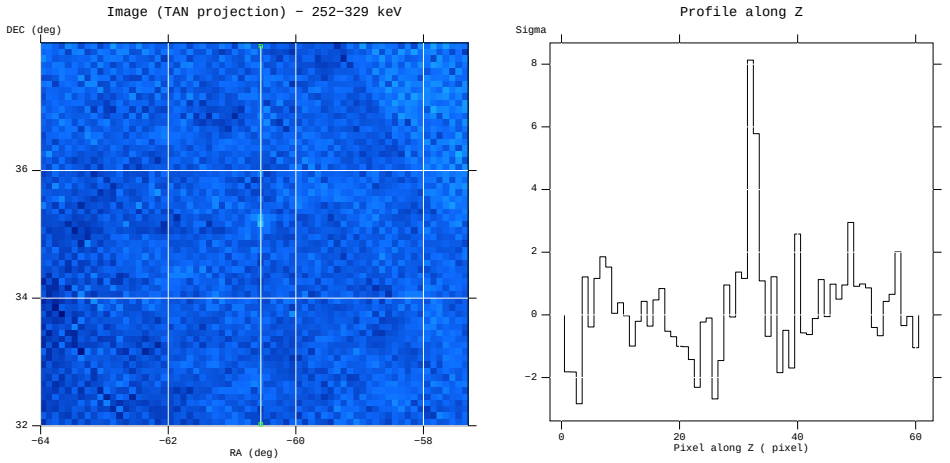

Figure 7: Cyg X–1 observed by PICsIT during the revolution 11 for 80 ks, dithering. Energy band 252 – 329 keV. Some background structures are clearly visible.

were several tests on the VETO configuration, the image is quite noisy, with fluctuations in the background. Nevertheless, the detection is clearly visible.

5 Timing

In February 2003, during the observation of the Crab, IBIS/PICsIT was set up to test the timing performances in the different modes of operation, i.e. photon–by–photon and spectral timing. Details on these observations and comparison with simultaneous observations with RXTE are published by Kuiper et al. (2003).

6 OSM

There are also three executables for the Operating Status Monitoring (OSM) in standard mode (spectral imaging, spectral timing) and photon–by–photon mode. They produce some standard products to monitor the instrument performances, that are shadowgrams, spectra and lightcurves for the whole detector, statistical analysis on the shadowgrams (mean value, maximum,

minimum, standard deviation). They are all working and stable. They are already used for the Consolidated Data Processing.

7 Other informations on IBIS/PICsIT

More informations on the in–flight performances of IBIS/PICsIT are available in the paper by Di Cocco et al. (2003). See also Malaguti et al. (2003b) for an analysis of the GRB021125. Here we show in Fig. 8 the fluxes of some bright sources compared with the sensitivity of IBIS/PICsIT.

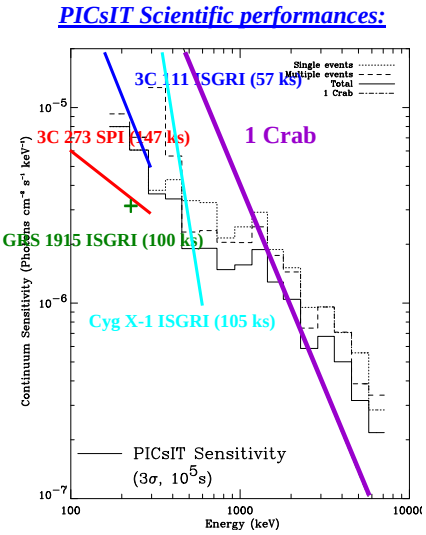

Figure 8: The flux of some bright sources detected with IBIS/ISGRI and SPI compared with the statistical sensitivity of IBIS/PICsIT (from Di Cocco et al. 2003). The fluxes have been taken from: Courvoisier et al. (2003) for 3C273, Bazzano et al. (2003) for Cyg X-1, J. Rodriguez (private communication) for GRS1915 + 105, and N. Gehrels (private communication) for 3C111.

Note: To make mosaics, it was used an executable originally developed by M. Revnivtsev to work on ISGRI data and modified by myself to use PICsIT images. With the kind permission of the author.

8 References

- Bazzano A., Paizis A., 2002, GCN1706
- Bazzano A., Bird A.J., Capitanio F., et al., 2003, A&A 411, L389
- Bouchet L., Roques J.P., Ballet J., Goldwurm A., Paul J., 2001, ApJ 548, 990
- Courvoisier T.J.-L., Beckmann V., Bourban G., et a., 2003, A&A 411, L343
- Del Santo M., Bazzano A., Bird A.J., et al., 2001, AIP Conference Proceedings **587**, 826.
- Di Cocco G., Caroli E., Celesti E., et al., 2003, A&A 411, L189
- Ferguson C., Barlow E.J., Bird A.J., et al., 2003, A&A 411, L19
- Goldwurm A., David P., Foschini L., et al., 2003, A&A 411, L223
- Gros A., Produit N., 2002, GCN1714
- Kuiper L., Hermsen W., Walter R., Foschini L., 2003, A&A 411, L31
- IBIS Calibration Team, *Scientific Performance Report*, IN.IB.IAS.RP.008/02, March 2002.
- Malaguti G., Bazzano A., Bird A.J., et al., 2003a, A&A 411, L173
- Malaguti G., Bazzano A., Beckmann V., et al., 2003b, A&A 411, L307
- Natalucci L., Bird A.J., Bazzano A., et al., 2003, A&A 411, L209
- Segreto A., Labanti C., Bazzano A., et al., 2003, A&A 411, L215
- Walter R., Favre P., Dubath P., et al., 2003, A&A 411, L25